Asia-Pacific Journal of Science and Technology: Volume: 28. Issue: 04. Article ID.: APST-28-04-11. Research Article

APST

Asia-Pacific Journal of Science and Technology

https://www.tci-thaijo.org/index.php/APST/index

Published by the Research and Graduate Studies Division,
Khon Kaen University, Thailand

Finite element analysis of CFRP-reinforced automotive hood under impact

Kunanon Sakkampang[1], Nirut Onsalung[1,*], Watcharayut Lumdoun[1] and Visit Junchuan[2]

[1]Department of Mechanical Engineering, Faculty of Industry and Technology, Rajamangala University of Technology Isan, Sakon Nakhon, Thailand
[2]Department of Mechanical Engineering, Faculty of Agriculture and Technology, Rajamangala University of Technology Isan, Surin, Thailand
[*]Corresponding author: nirut.on@rmuti.ac.th

Received 11 March 2022
Revised 26 April 2022
Accepted 8 June 2022

Abstract

This study aimed to explore the crashworthiness characteristics of carbon fiber reinforced plastics (CFRP) composite materials, based on the strength and energy absorption capacity. The specimen was an automotive hood which was tested numerically by using impact tests and finite element modeling simulation. The carbon fiber was reinforced by plastics with different orientations including $[0/90]_2$, $[0/90]_3$, $[0/90]_4$, $[45/-45]_2$, $[45/-45]_3$, and $[45/-45]_4$ which were tested under impact using drop hammer tower testing machine. The results revealed that the maximum load occurred with the $[0/90]_4$ carbon fiber layers. With the $[0/90]_4$ and $[45/-45]_4$ carbon fiber layers, the specimens showed an increase in the mean load. In terms of energy absorption, findings revealed that $[45/-45]_4$ specimen had higher value when the numbers of fibers were increased, whereby the absorbed energy was 1.13 kNm. The results from the impact test were relevant to the results of the finite element modeling simulation which could confirm the results of the impact tests.

Keywords: Composite materials, Finite element analysis, Impact test, CFRP

1. Introduction

Composite materials are an alternative option in a wide variety of applications today. Carbon fiber is most commonly used in the aerospace industry, automotive, wind power and sports equipment industries because it is a low-density material with high strength, excellent fatigue resistance and excellent corrosion resistance [1-5]. Carbon fiber is commonly used as a replacement for heavy-duty materials such as steel, aluminum, and magnesium [6,7]. Therefore, designers have found a way to change materials from metal to plastic reinforced by carbon fibers, which have important properties such as lightweight, high hardness, high energy absorption capacity, fatigue resistance, and corrosion resistance. The deformation behavior of carbon fiber material is highly flexible and this is beneficial for designs that require rigidity [8], therefore, carbon fiber materials have been used in many research areas, such as automotive parts [6], concrete [9], aerospace materials [10].

There are many interesting studies on the industrial applications of carbon fiber especially the use of finite programming to help in the analysis. This is because the use of finite element programming reduces material cost and also enables design. The results of the experiments are analyzed accurately and the use of the Finite element analysis (FEA) program in the analysis of composite materials is increasingly being employed [11]. In the past, there have been research studies on car hoods made of many composite materials as follows; Ahad Torkestani et al. [12] studied the influence of fibers and the impact position on the head under impact. The engine hood was made of 4 different materials including aluminum, steel, carbon fiber with epoxy and glass fiber with epoxy. The composition was determined to be wrapped and placed at an angle of $[0]_8$, $[90]_8$, $[0/90/0/90]_2$, and $[-45/0/45/90]_2$. Child and adult head models had semi-circular shape with diameters of 130 and 165 mm and mass of 2.5 and 4.5 kg, respectively. The speed of impact test between the head and the engine hood of child and adult was 40 km/h. The results showed that the engine hood of composite materials helped reduce head injury (HIC) by 46.8% compared with steel.

Shojaeefard et al. [13] studied and developed the finite element model with collisions between a human head model and an engine hood. The internal engine hood had 5 different styles including standard factory, semicircle, cone, wave, and combination between semi-circle and cone. The engine hood was tested under the standard of european enhanced vehicle-safety committee (EEVC) and working group 17 (WG17). The results showed that the newly improved engine hood had more energy absorption, acceleration and HIC values compared to the factory standard and was lighter by 12.7%. Ahmed et al. [14] used finite element model to study an engine hood made from carbon and epoxy materials for the safety of pedestrians. The engine hood was made of T300 carbon fiber material and epoxy type RIMH 137. The angles of the fiber were $[0/90/+45/-45]_2$ $[[0/90/+45/-45]_2$, and 0/90, $[0/90]_4]$, the thickness of the engine hood was 1.0 to 2.5 mm. european new car assessment programme (Euro-NCAP) standard impact testing with speed of 11.1 m/s was done by using the finite element model ABAQUS/explicit program. The model results showed that all engine hoods and engine hood angles $[0/90/+45/-45]_2$ could reduce HIC damage.

Kim et al [15] studied the composite structure of an engine hood under impact. The engine hood was made from two types of composite materials;carbon with epoxy and hybrid of carbon fibers and glass fibers with epoxy. The carbon fiber wrapping was angled at [0/-45/ 45/45/-45/0], [75, 15, 0] for top cover, and $[-15, 0, 15]_2$ for bottom cover and hybrid of carbon fibers and glass fibers with epoxy $[45, 75, 60]_2$ for top cover, and $[-0, -30, -30]_2$ for bottom cover. Conclusion from the model revealed that carbon with epoxy and hybrid had lower HIC and weight than the engine hood with aluminum material. Huang and Yang [16] studied the suitability of an auto lifted engine hood by Euro-NCAP standard impact testing with two impactors which were EEVC WG17 adult head form model and human head FEA model test with a mass of 5.59 kg. The impact velocity was 9.94 m/s with tilt angle of 45 degrees. The results showed that finite element simulation accurately predicted the results.

Therefore, this study concentrated on multiple layers of carbon fiber sheets to produce a car hood. This research aimed to study the technique of forming automotive parts with carbon fiber-reinforced with the ability to absorb energy. The strength of the developed automotive parts such as impact resistance and material strength, the effect of carbon fiber angle, shape, and damage pattern were investigated. The result of this study suggests appropriate carbon fiber layers to produce light-weight materials that can absorb higher energy leading to the production of automotive parts or bogie parts for high-speed trains, which is an important strategy for the country at the moment and can be extended to commercial production in the future.

2. Materials and methods

2.1 Patterns of carbon fiber used in the experiment

When analyzing a car hood model, it is important to consider how accurately and reliably the model predicts. Carbon fiber sheets were selected for the study of carbon fiber reinforced plastics (CFRP). In this study and similar to the research of Ueda et al. [17] and Mamalis et al. [18], unidirectional pattern which is characterized by the orientation of the fibers in one line, was used as shown in Figure 1. To compare with the FEA model, the carbon fiber sheets were formed as circular tubes as this did not have complicated structure and it was easy to form a model. The method formed the material into a circular tube with many layers of carbon fiber overlapping and an impact test was performed using an impact tester with a hammer head dropped down against an aluminum tube and carbon fiber, similar to the research of Junchuan and Thinvongpituk [19]. The weight of the hammer used to hit the specimen was 30 kg at 2 m impact height (V= 6.26 m/s) to test the resulting load. A model was then created according to the experimental conditions and the results compared first to find out whether there was a difference between the experimental results and the model. The various properties of the material were tested by the Mechanical Testing Laboratory of the National Metal and Materials Technology Center (MTEC) The results of this test showed that the model results were similar to the laboratory results. Therefore, the researcher created a model of a car hood and analyzed it using FEA methodology to confirm that the model analysis approach was accurate according to the research goals.

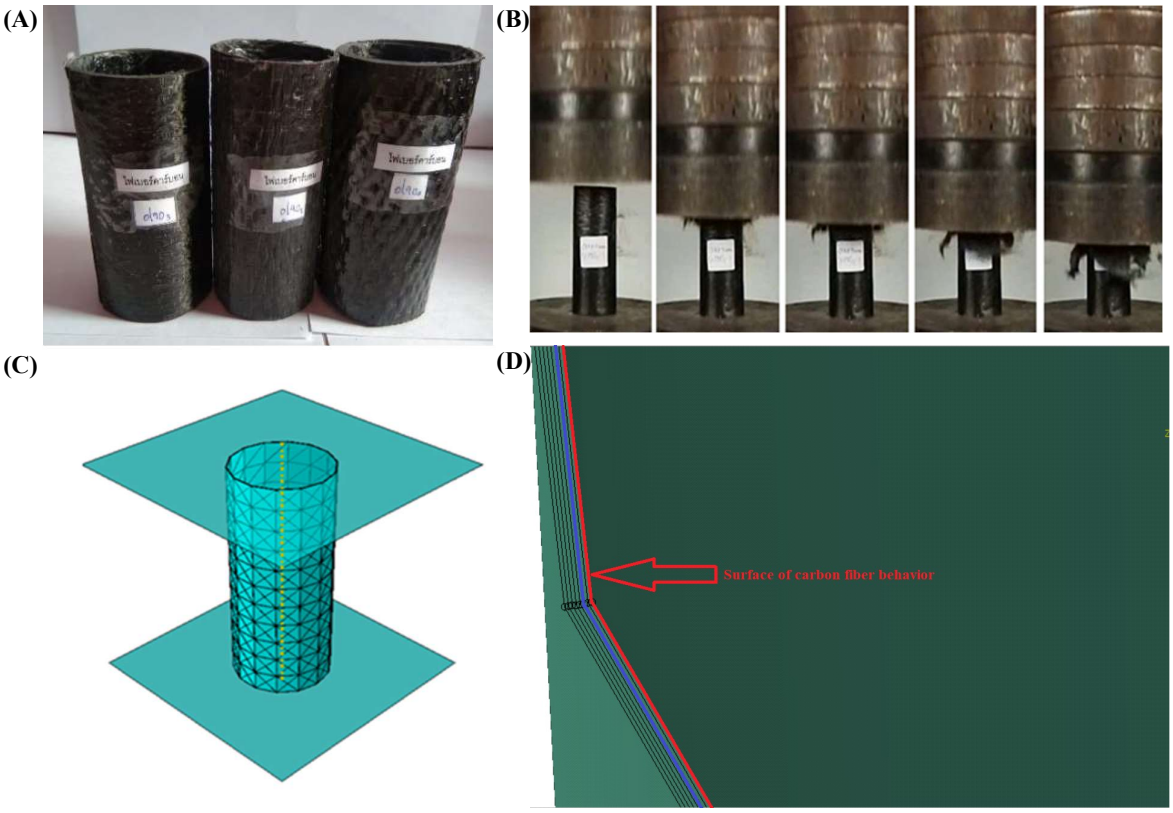

Figure 1 Specimens and prototype analysis of carbon fiber tubes for making a car hood (A) Carbon fiber tube used in impact testing (B) Damage of the carbon fiber tube (C) Configuration of the model for FEA (D) Layer arrangement of the component for FEA.

In the impact test of the carbon fiber prototype tube, comparative models were tested and analyzed in 6 different ways: $[0/90]_2$, $[0/90]_3$, $[0/90]_4$, $[45/-45]_2$, $[45/-45]_3$, and $[45/-45]_4$. The results of both experimental and simulation analyses are shown in the graph in Figure 2. It was found that the values of the experimental model results and the simulation model were in the same direction as a mountain-like curve. When the results of the maximum load of the experimental results and the model from Table 1 were compared, it was found that the difference between the experiment and the FEA model was 12.721%, which was an acceptable value able to imply the reliability of generating hood model for analysis using the FEA model alone.

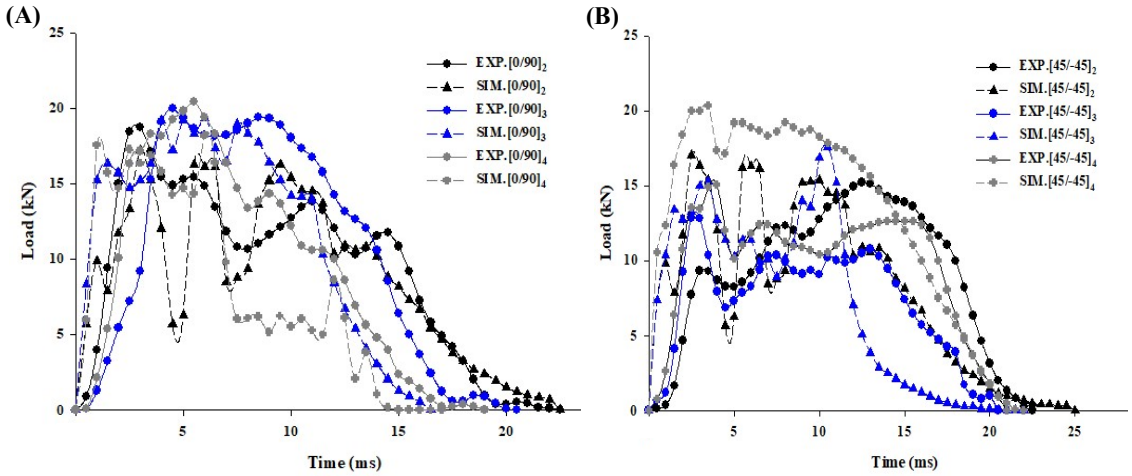

Figure 2 The results of the experimental and simulation analyses of the carbon fiber prototype tube; (A) Comparison of experimental results and the model of the component with [0/90] fiber Orientation, and (B) Comparison of experimental results and the model of the component with [45/-45] fiber Orientation.

Table 1 The difference between the experimental and FEA analyses of prototype tubes made of carbon fiber material.

Type	P_{max} (kN) Experimental	P_{max} (kN) Simulation	Difference (%)
$[0/90]_2$	18.694	17.229	7.839
$[0/90]_3$	19.948	19.303	3.236
$[0/90]_4$	20.383	18.156	10.925
$[45/-45]_2$	15.223	17.036	11.910
$[45/-45]_3$	16.882	17.588	4.183
$[45/-45]_4$	18.022	20.314	12.721

For the damage of carbon tubes upon impact, two types of tubes were taken, 4-layer carbon fiber tubes 0/90 and 45/-45 (Figure 3), as the 2- and 3-layer tubes exhibited damage behavior. By studying the structural behavior when subjected to loads for a period of time, it was found that the 0/90 tube had initial damage characteristics at the top end of the model tube. After that, the model tube collapsed. In the case of 45/-45, the element ruptured or ruptured along the fibers until the tube collapsed. The experimental part showed that there was damage at the top end of the pipe. The 45/-45 pipe revealed that the fibers were torn and flared apart until the end of the collapse of the workpiece pipe. Similar characteristics were found when both 0/90 and 45/-45 pipe damage processes between the experiment and the FEA model were compared.

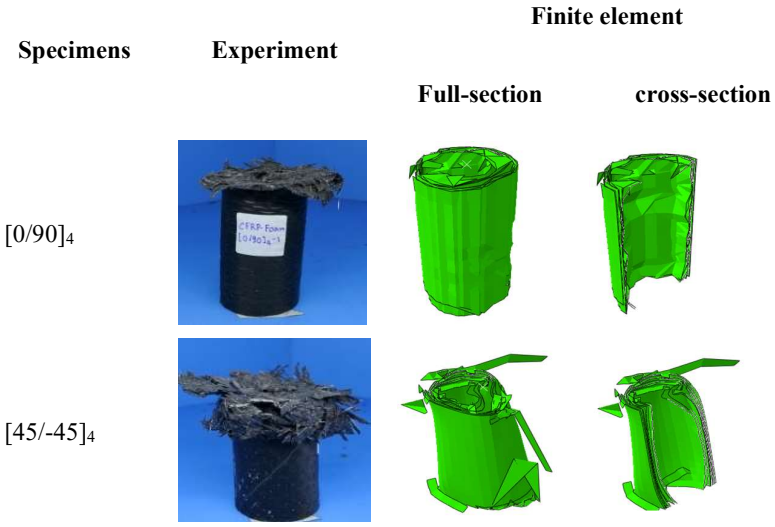

Figure 3 A comparison of the damage behavior of carbon tubes upon impact in the experiment and FEA model.

2.2 Mechanical properties

The mechanical properties of the composite materials used in this research were obtained from testing the actual materials as shown in Tables 2-5. The tensile and compression machine used in the research was Universal Testing Machine Dynamic Type Instron model 8801 capacity of compression 100 kN, as shown in Figure 4. The mechanical properties of specimens were tested from the laboratory of National Metal and MTEC. The machine working principle was performed by using the hydraulic to drive the test head to move in order to create a force on the specimens under a computer-controlled system and measured by a load cell. The deformation of the specimen was measured by the moving distance of the actuator or extensometer. The tensile test was in accordance with a standardized test of american society for testing and materials (ASTM) D 3039 [20] by orientation and stacking sequence of fibers as follows $[0]_4$, $[45]_4$ and $[90]_4$ degrees in one direction. The specimen had a width of 25 mm and length of 250 mm. The velocity used in the test was 10 mm/min. The results of the testing are shown in Tables 1 to 3. Compression resistance testing along the fibers by orientation and stacking sequence of fibers was performed as follows $[0]_4$, $[45]_4$ and $[90]_4$ degrees as shown in Figure 5. The width was 25 mm, the length was 120 mm and the velocity used in the test was 10 mm/min. The results of this tests are shown in Tables 2-4. In the case of testing the resistance of the strands separated by the strands in unidirectional 0 degrees, the angle of the fibers along the longitudinal or $[0]_4$ degrees had a width of 25.00 mm, a length of 150 mm and a length of

separation of 100 mm, the velocity used in the test was 10 mm/min. The maximum stress and energy fracture values were 2.75 MPa and 0.051867 MJ/m^2, respectively, as shown in Table 5.

Table 2 Elastic properties and densities of carbon.

Property	Description	Value
ρ	Density (kg/m^3)	1500
E_{11}	Young's modulus in longitudinal fiber direction (GPa)	66.34
E_{22}	Young's modulus in transverse direction (GPa)	7.152
G_{12}	In-Plane shear modulus (GPa)	9.653
G_{23}	Out of Plane shear modulus (GPa)	2.458
υ_{12}	Poisson's ratio	0.269
υ_{23}	Poisson's ratio	0.455

Table 3 Material properties for maximum strength.

Property	Description	Value (MPa)
X_T	Longitudinal tensile strength	1142.14
X_C	Longitudinal compressive strength	263.78
Y_T	Transverse tensile strength	18.23
Y_C	Transverse compressive strength	35.25
S_{12}	Longitudinal Shear strength	28.83
S_{23}	Transverse Shear strength	30.50

Table 4 Material features of fracture energy.

Property	Description	Value (MJ/m^2)
G_t	Longitudinal tensile Fracture Energy	0.4911
G_c	Longitudinal compressive Fracture Energy	0.0639
G_t	Transverse tensile Fracture Energy	0.0006
G_c	Transverse compressive Fracture Energy	0.0065

Table 5 Material properties of damage mechanisms of the carbon fibers.

Property	Description	Value
ρ	Density (kg/m^3)	1500
t_n	Damage initiations (MPa)	2.7512
G_n	Energy Fracture (MJ/m^2)	0.0518

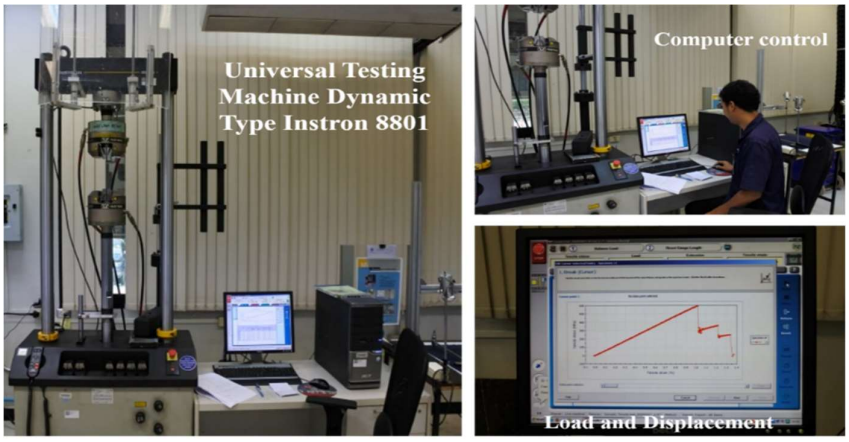

Figure 4 Universal Testing Machine Dynamic Type Instron 8801.

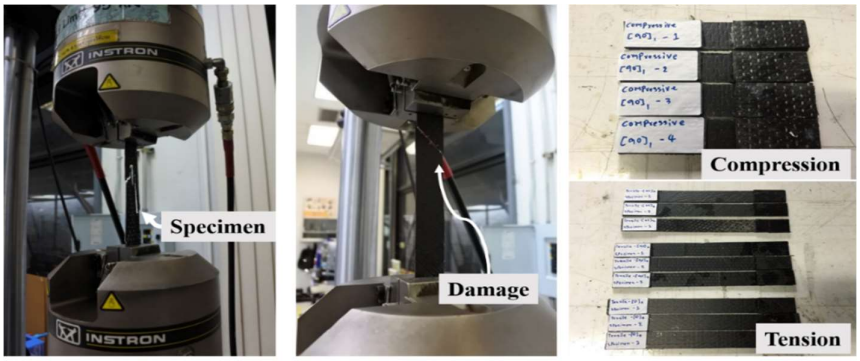

Figure 5 The specimen-gripping for tensile and compression testing.

2.3 Composite layup of model

This research studied the influence of angle t on the engine hood (Figure 5) shows the carbon fiber reinforced plastics had different patterns of orientations angle with 6 models: $[0/90]_2$, $[0/90]_3$, $[0/90]_4$, $[45/-45]_2$, $[45/-45]_3$, and $[45/-45]_4$ degrees. The maximum load, average load, and energy absorption of each pattern of orientation angles are shown in Table 6. The direction in the ABAQUS/explicit program defines the coordinate system which sets the X axis to the longitudinal model and the Y axis to the transverse model as shown in Figure 6, showed that the coordinate system of the axis consisted of axes 1, 2 and n. Axis number 1 is the angle direction of the fibers along the longitudinal of 0°, and axis number 2 is the angle direction of the fibers along the transverse of 90° and the n-axis is normal.

Table 6 Maximum load, Average load, and Energy absorption.

Type	Maximum load (kN)	Mean load (kN)	Time (s)	Displacement (m)	Energy absorption (kN/m)
AL	10.352	3.435	0.022	0.242	0.831
$[0/90]_2$	13.754	4.237	0.019	0.209	0.885
$[0/90]_3$	19.996	8.306	0.010	0.110	0.914
$[0/90]_4$	31.523	8.867	0.011	0.121	1.073
$[45/-45]_2$	12.341	4.778	0.019	0.209	0.999
$[45/-45]_3$	20.264	8.280	0.012	0.132	1.093
$[45/-45]_4$	26.103	8.547	0.012	0.132	1.128

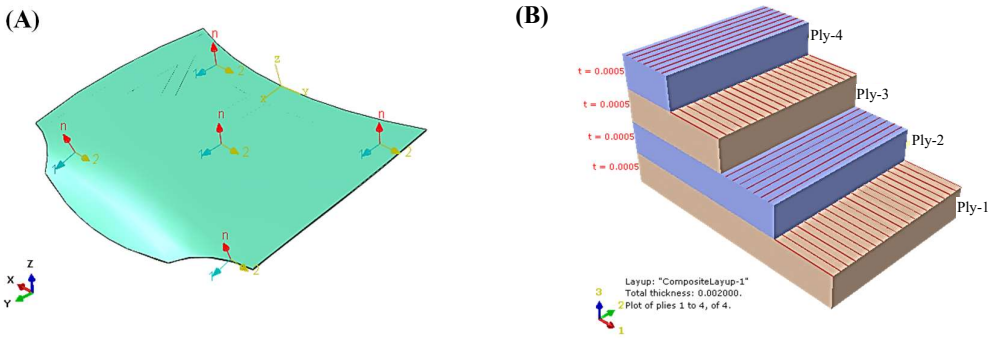

Figure 6 The orientation of fibers composite layup (A) the orientation of the fibers and definition of a secondary axis Coordinate System and (B) the number of layers and the orientation of the fibers ply stack plot.

2.4 The FEA model of the car hood

FEA is widely used for predicting how a product reacts to real-world forces which help determine to composite optimization and to obtain the best value of compliance similar to that of the original objects [21]. A previous study was conducted by using FEA to determine HIC of a composite car hood [22] with the focus on shock absorption from the impact. In this study, FEA was used to predict shock absorption of the specimens which were carried out following the method of Acanfora et al. [23]. Model components were created with 4 parts:

top cover, bottom cover, impactor and supporter (Figure 7). A model of engine hood was assembled and bonded together. The impactor was defined as a rigid body with a diameter of 150 mm and 300 mm of height. The supporter was a rigid body with a width of 700 mm and a height of 100 mm, the boundary condition of the model is shown in Figure 8. The model was determined according to the actual experimental conditions. The details were as follows; the impactor had a mass of 4.8 kg with independent maximum falling speed of 11 m/s and it could only move up or down on Y axis. The supporter was defined as the load cell base, which was fixed and recorded the load (RF2 reaction force along the Y axis). The supporter of this model was determined by the U1, U2, U3, UR1, UR2, and UR3 which were set at 0. The mesh and element of the model consisted of 4 parts with impactor and supporter being rigid bodies without damage. The element size was 70 mm with type R3D4: A 4-node 3-D bilinear rigid quadrilateral, where R is the rigid body, 3D is three dimensional and 4 is the four nodes. The element size of carbon engine hood was 17.5 mm with type o S3R elements: A 3-node triangular thin or thick shell, finite membrane strain, where S is the thin wall structure or thin shell (Shell), 4 is the four nodes and R is the reduced integration. The smallest element size of the carbon engine hood could perform FEA model and display a better damage distribution than a larger element size.

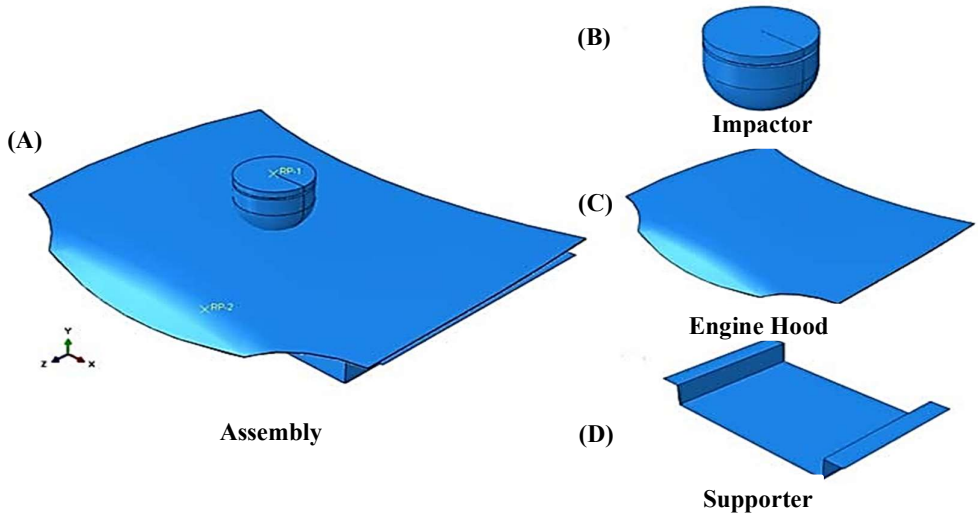

Figure 7 Structural model (A) Complementary overview of the hood model (B) Impactor (C) the hood and (D) Supporter.

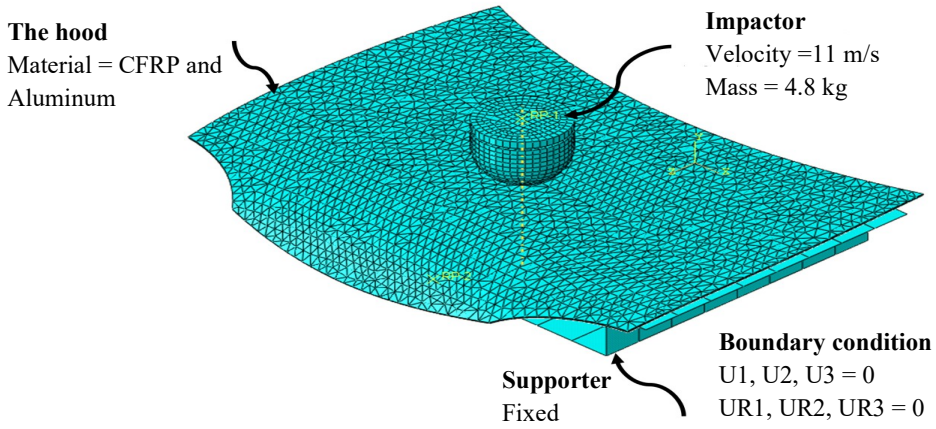

Figure 8 Model of the engine hood and definition of boundary conditions.

3. Results

Figure 9 shows that the damage process of the engine hood of CFRP which was wrapped in fibers $[45/-45]_4$ had a total duration of impact testing as 0.0200 seconds. Initially, the impactor was in contact with the engine hood of CFRP at 0.000 seconds which caused damage and widened the entire surface. This time period caused

the engine hood of CFRP to resist the load from the impactor, resulting in the maximum load during 0.0025 seconds. The engine hood of CFRP instantly collapsed and caused low load at a period of 0.0075 - 0.0125 seconds. The impactor was reflected back to the end of the testing process at 0.0125 - 0.0200 seconds.

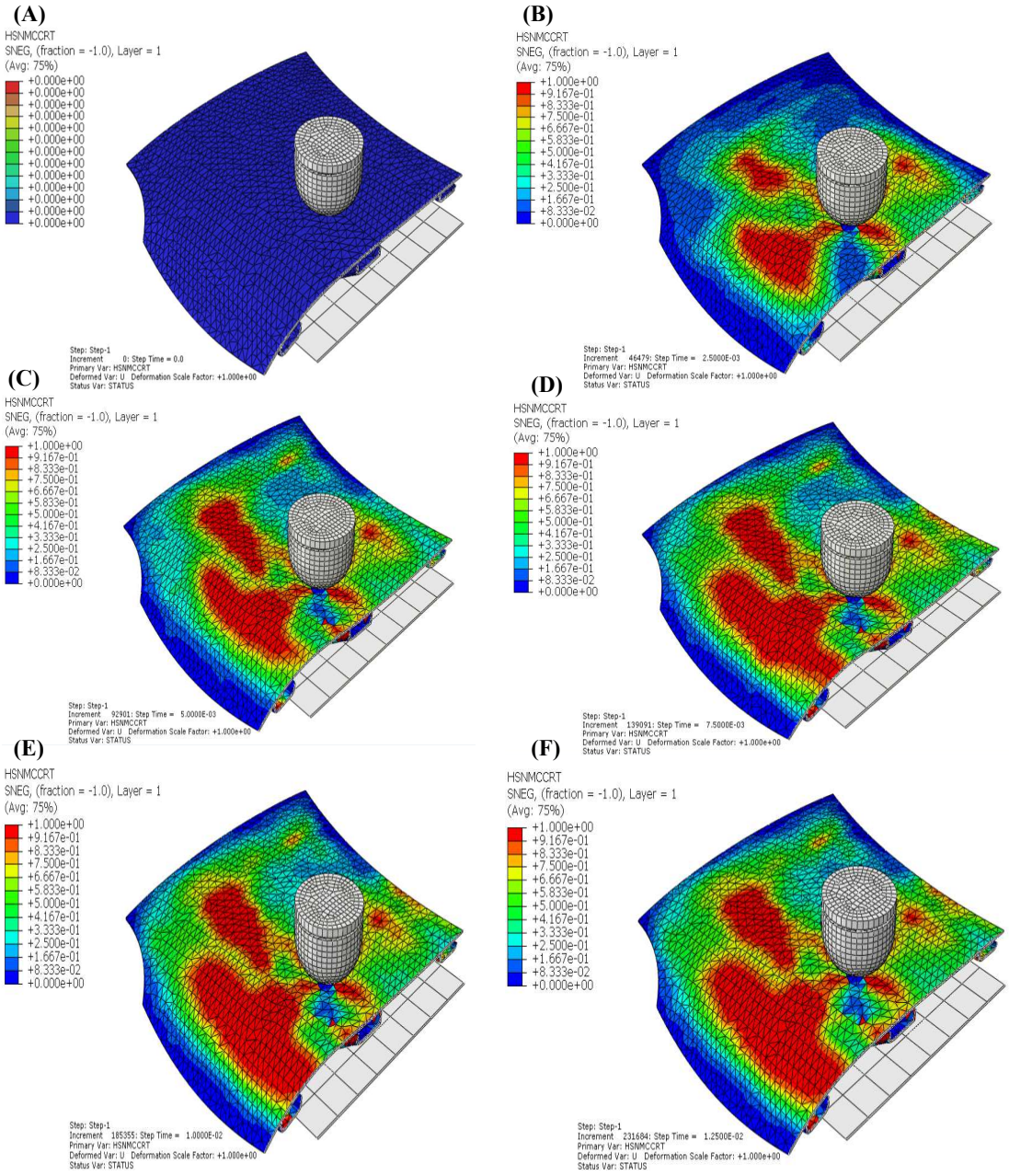

Figure 9 The damage process of the engine hood of CFRP wrapped in fibers [45/-45]4. (A) Time = 0.0005 s (B) Time = 0.0025 s, (C) Time = 0.005 s, (D) Time = 0.0075 s, (E) Time = 0.0100 s, (F) Time = 0.0125 s, (G) Time = 0.0150 s, (H) Time = 0.0175 s, (I) Time = 0.0200 s.

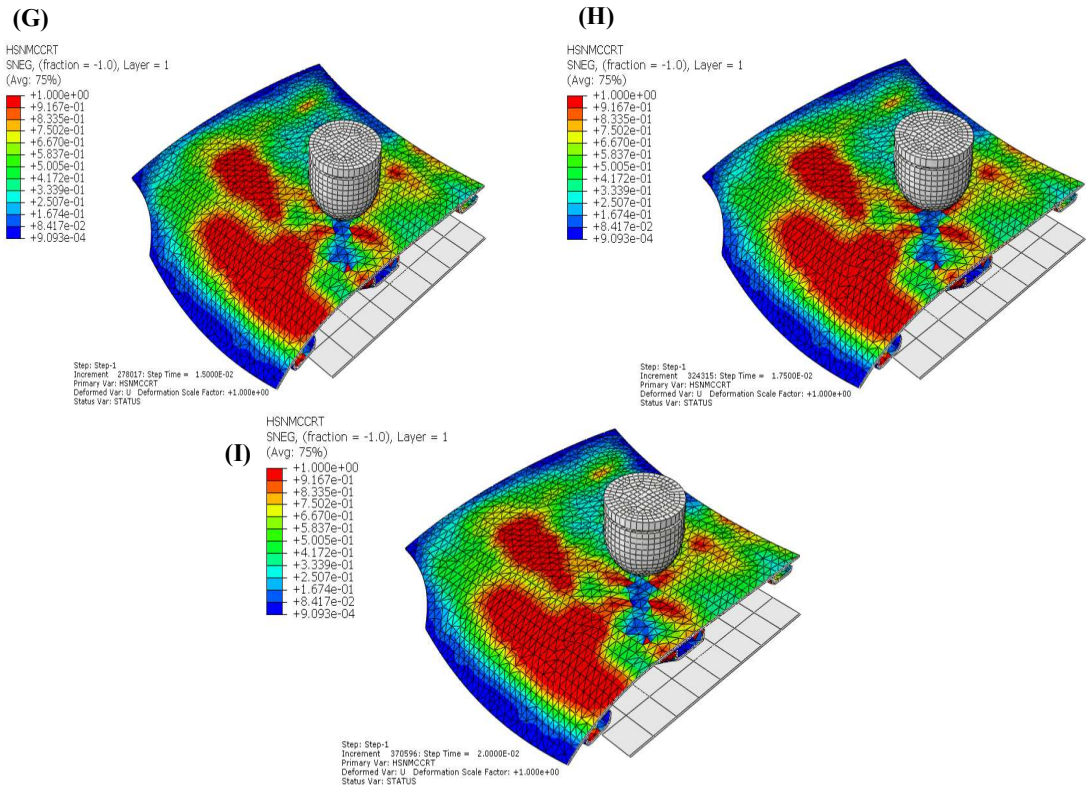

Figure 9 (Continued) The damage process of the engine hood of CFRP wrapped in fibers [45/-45]4. (A) Time = 0.0005 s (B) Time = 0.0025 s, (C) Time = 0.005 s, (D) Time = 0.0075 s, (E) Time = 0.0100 s, (F) Time = 0.0125 s, (G) Time = 0.0150 s, (H) Time = 0.0175 s, (I) Time = 0.0200 s.

3.1 Damage of the engine hood

Figure 10 shows the result of the engine hood model made of aluminum material under axial impact which shows stress distribution from von Misses stress in the form of color stress. It was found that the stress distribution characteristics were circular throughout the surface. The engine hood area received the maximum stress at 188.6 MPa while the lowest stress occurred at the edge of engine hood at 1.093 MPa.

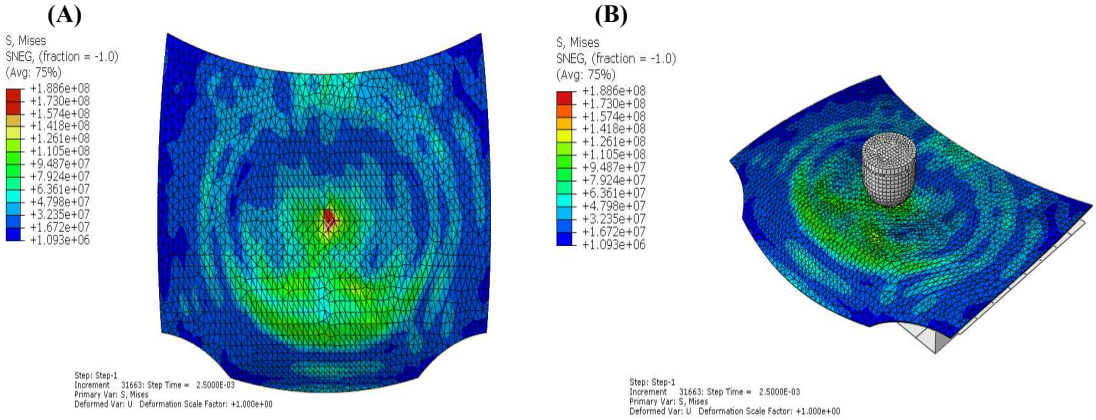

Figure 10 The results of the von Mises stress of engine model made of aluminum material under axial impact (A) The von Misses stress (Top View), (B) The von Misses stress (Isometric view) with hammer, (C) The von Misses stress (Isometric view).

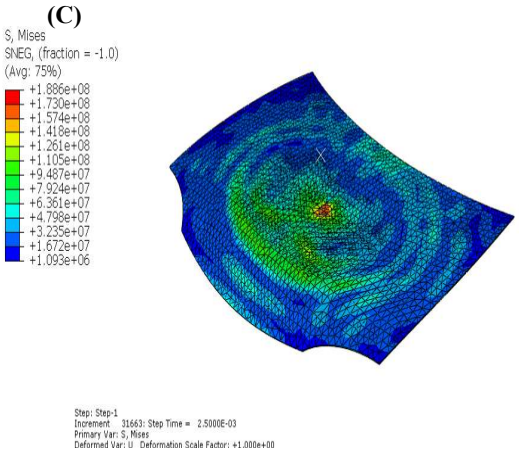

Figure 10 (Continued) The results of the von Mises stress of engine model made of aluminum material under axial impact (A) The von Misses stress (Top View), (B) The von Misses stress (Isometric view) with hammer, (C) The von Misses stress (Isometric view).

Figure 11 shows the results of the stress distribution of fiber damage and plastic damage (Matrix) on the engine hood of CFRP with different fiber angles under axial impact. The results of the Von Misses stress of the engine hood of CFRP with the fibers ply angles of $[0/90]_2$, $[0/90]_3$, and $[0/90]_4$ degrees showed that an increase in the number of fibers layer led to an increase in the stress to 291.0, 349.0 and 391.0 MPa, respectively, whereby the maximum stress occurred at the center of the engine hood of CFRP, after which the stress distribution throughout the area tended to decrease to the edge of the engine hood of CFRP. The fiber compressive damage of the engine hood of CFRP showed that at the ply angles of $[0/90]_2$, $[0/90]_3$ and $[0/90]_4$ degrees, the fiber damage tended to increase, respectively, which distributed the damage onto the longitudinal and transverse characteristics of the engine hood of CFRP. This was due to the influence of the fiber angles [0/90] degrees and the matrix compressive damage which showed that the damage tended to increase accordingly.

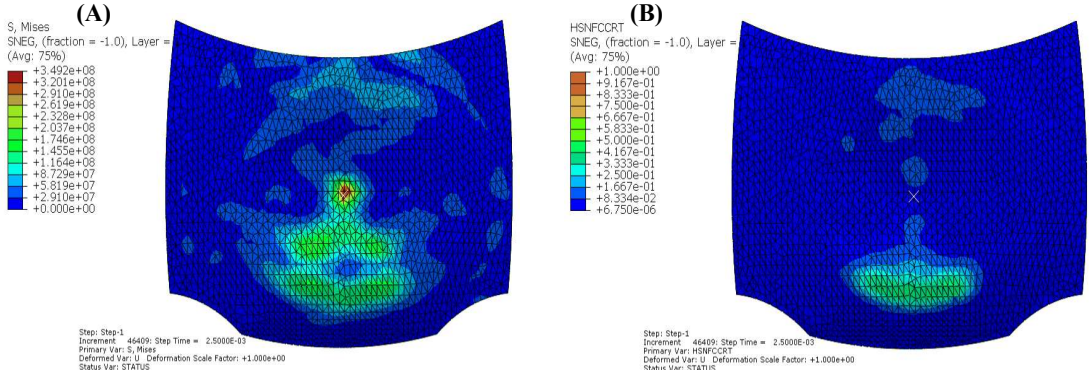

Figure 11 The results of the stress distribution, fiber damage and plastic damage (Matrix) of the engine hood of CFRP wrapped in fibers under axial impact. (A) von Mises stress of ply angles [0/90]2 degrees, (B) Fiber compressive damage of ply angles [0/90]2 degrees, (C) Matrix compressive damage of ply angles [0/90]2 degrees, (D) von Mises stress of ply angles [0/90]3 degrees, (E) Fiber compressive damage of ply angles [0/90]3 degrees, (F) Matrix compressive damage of ply angles [0/90]3 degrees, (G) von Mises stress of ply angles [0/90]4 degrees, (H) Fiber compressive damage of ply angles [0/90]4 degrees, (I) Matrix compressive damage of ply angles [0/90]4 degrees, (J) von Mises stress of ply angles [45/-45]2 degrees, (K) Fiber compressive damage of ply angles [45/-45]2 degrees, (L) Matrix compressive damage of ply angles [45/-45]2 degrees, (M) von Mises stress of ply angles [45/-45]3 degrees, (N) Fiber compressive damage of ply angles [45/-45]3 degrees, (O) Matrix compressive damage of ply angles [45/-45]3 degrees, (P) von Mises stress of ply angles [45/-45]4 degrees, (Q) Fiber compressive damage of ply angles [45/-45]4 degrees, (R) Matrix compressive damage of ply angles [45/-45]4 degrees.

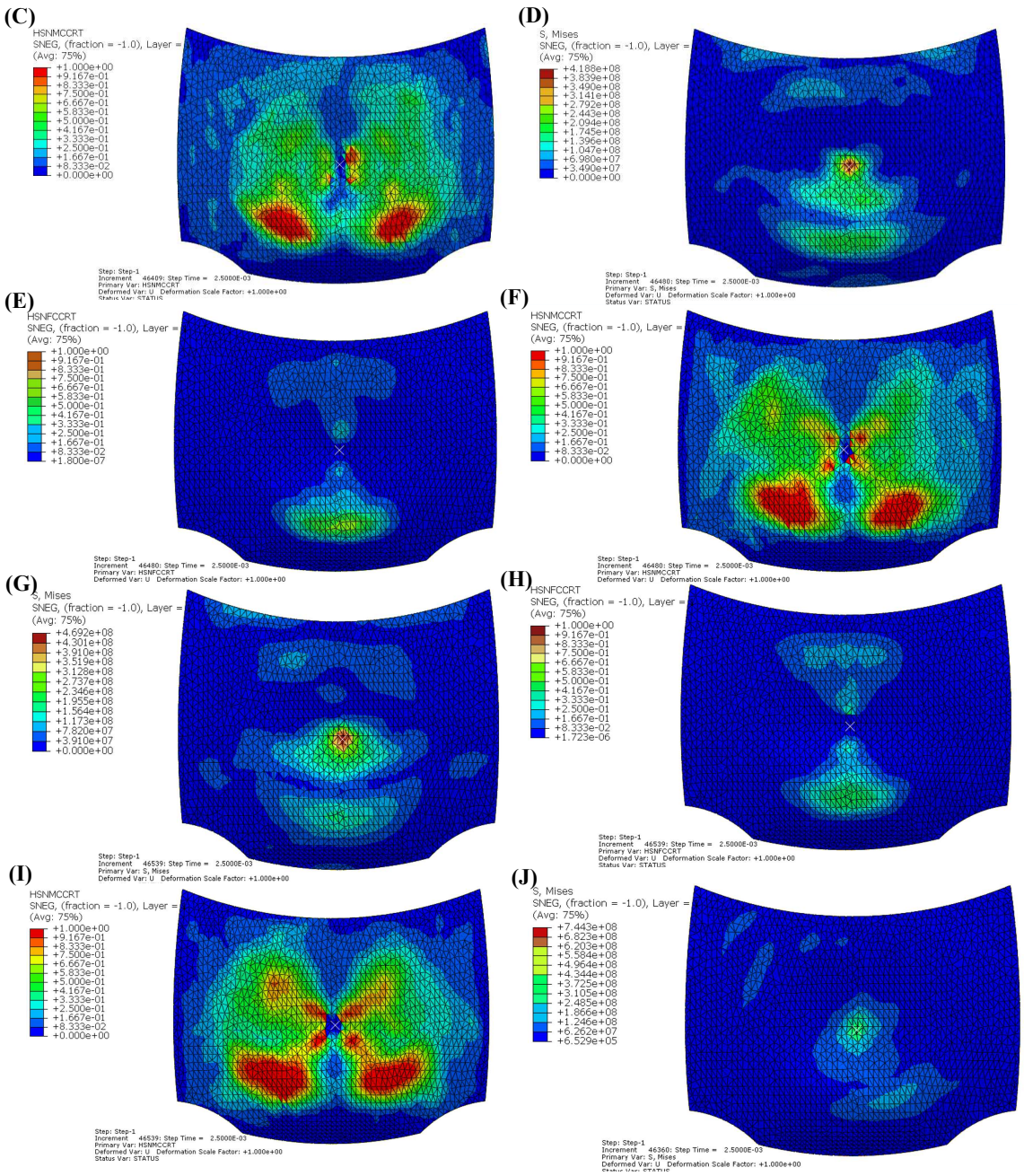

Figure 11 (Continued) The results of the stress distribution, fiber damage and plastic damage (Matrix) of the engine hood of CFRP wrapped in fibers under axial impact. (A) von Mises stress of ply angles [0/90]2 degrees, (B) Fiber compressive damage of ply angles [0/90]2 degrees, (C) Matrix compressive damage of ply angles [0/90]2 degrees, (D) von Mises stress of ply angles [0/90]3 degrees, (E) Fiber compressive damage of ply angles [0/90]3 degrees, (F) Matrix compressive damage of ply angles [0/90]3 degrees, (G) von Mises stress of ply angles [0/90]4 degrees, (H) Fiber compressive damage of ply angles [0/90]4 degrees, (I) Matrix compressive damage of ply angles [0/90]4 degrees, (J) von Mises stress of ply angles [45/-45]2 degrees, (K) Fiber compressive damage of ply angles [45/-45]2 degrees, (L) Matrix compressive damage of ply angles [45/-45]2 degrees, (M) von Mises stress of ply angles [45/-45]3 degrees, (N) Fiber compressive damage of ply angles [45/-45]3 degrees, (O) Matrix compressive damage of ply angles [45/-45]3 degrees, (P) von Mises stress of ply angles [45/-45]4 degrees, (Q) Fiber compressive damage of ply angles [45/-45]4 degrees, (R) Matrix compressive damage of ply angles [45/-45]4 degrees.

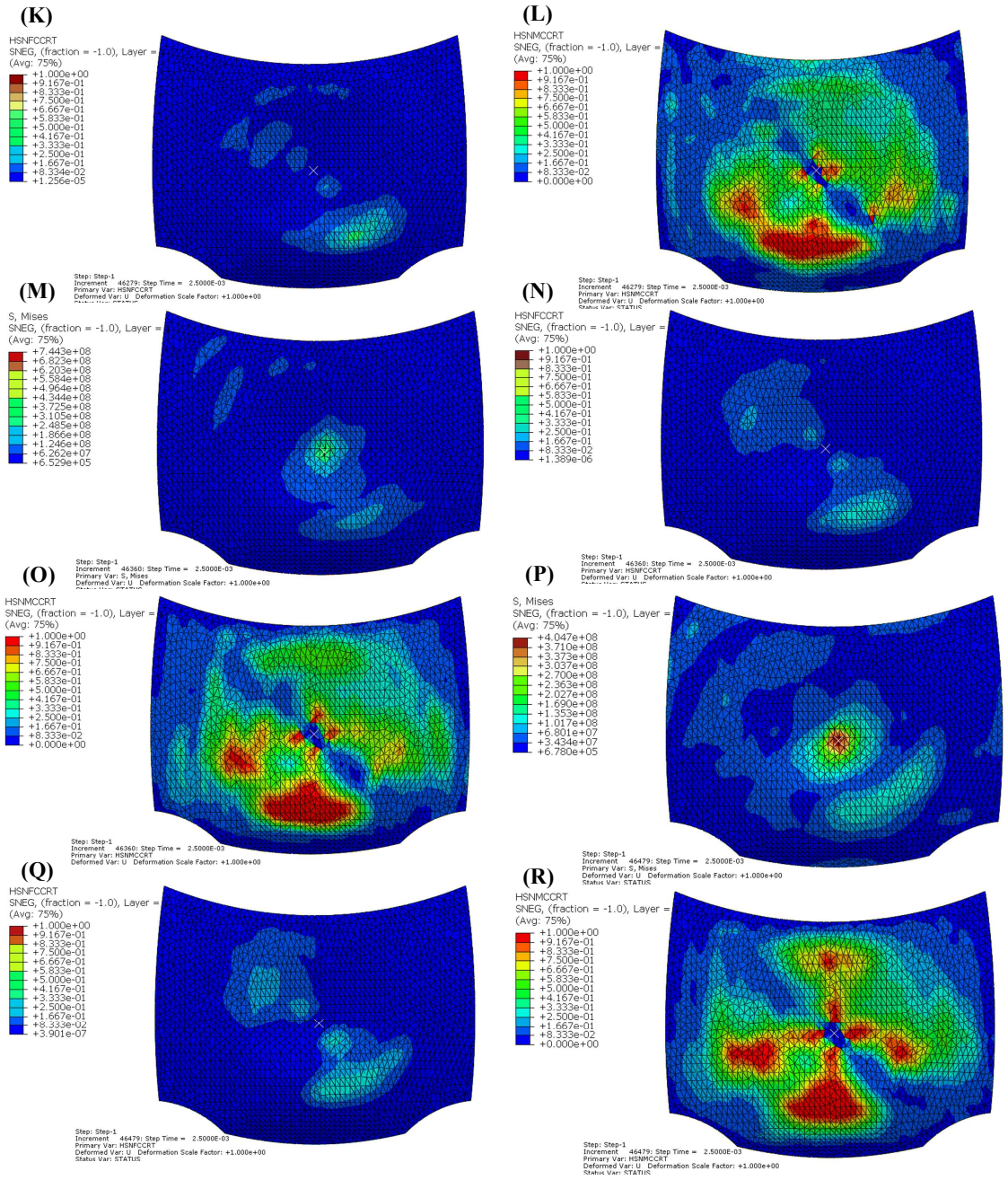

Figure 11 (Continued) The results of the stress distribution, fiber damage and plastic damage (Matrix) of the engine hood of CFRP wrapped in fibers under axial impact. (A) von Mises stress of ply angles [0/90]2 degrees, (B) Fiber compressive damage of ply angles [0/90]2 degrees, (C) Matrix compressive damage of ply angles [0/90]2 degrees, (D) von Mises stress of ply angles [0/90]3 degrees, (E) Fiber compressive damage of ply angles [0/90]3 degrees, (F) Matrix compressive damage of ply angles [0/90]3 degrees, (G) von Mises stress of ply angles [0/90]4 degrees, (H) Fiber compressive damage of ply angles [0/90]4 degrees, (I) Matrix compressive damage of ply angles [0/90]4 degrees, (J) von Mises stress of ply angles [45/-45]2 degrees, (K) Fiber compressive damage of ply angles [45/-45]2 degrees, (L) Matrix compressive damage of ply angles [45/-45]2 degrees, (M) von Mises stress of ply angles [45/-45]3 degrees, (N) Fiber compressive damage of ply angles [45/-45]3 degrees, (O) Matrix compressive damage of ply angles [45/-45]3 degrees, (P) von Mises stress of ply angles [45/-45]4 degrees, (Q) Fiber compressive damage of ply angles [45/-45]4 degrees, (R) Matrix compressive damage of ply angles [45/-45]4 degrees.

The von Misses stress of the engine hood of CFRP wrapped in Ply angles $[45/-45]_2$, $[45/-45]_3$, and $[45/-45]_4$ degrees found that the stress value tended to increase to 242.6, 310.5 and 371.0 Mpa, respectively. The stress distribution characteristics were found in an oblique direction in the direction of the fibers of the engine hood of CFRP. The results of the fiber compressive damage of the engine hood of CFRP wrapped in ply angles $[45/-45]_2$, $[45/-45]_3$, and $[45/-45]_4$ degrees showed that fiber damage tended to increase, respectively, and the characteristics were in an oblique direction of the engine hood of CFRP. The matrix compressive damage showed the maximum damage in the center and distributed throughout the engine hood of CFRP. The damage in the oblique direction of the engine hood of CFRP was in the same direction as the fiber orientation.

3.2 Maximum and mean load

When the engine hood was tested with sudden impact load, this caused deformation by collapsing and affecting energy absorption behavior which was reflected in the form of load and time graph (Figure 12A) shows the graph of load and time of the engine hood in all 7 cases. The relationship between load and time was recorded in the graph t which showed an initial upward trend in linear form and after which the graph alternated up and down trends until the end of the impact (Figure 12B) shows the maximum load and the mean load. The results from the FEA model showed that the maximum load increased with an increase in the number of carbon fiber layers accordingly, as caused by the increased influence of carbon fibers and the thickness of the engine hood. In addition, it was found that the angle of the carbon fibers [0/90] of 4, 6 and 8 layers affected different loads, which was caused by the 90-degree angle of the engine hood receiving the initial load, which served to distribute the load across the area and for the 0 degree angles onto the longitudinal engine hood as the main load which served to resist deflection and distribute the load of the engine hood along the length affected to receive the maximum and mean load.

The effect of stacking sequence of carbon fibers angles [45/-45] of 4,6 and 8 layers showed that the maximum and mean load tended to increase with an increase in the number of fibers layers caused by the influence of number of layers and thickness. The angles of the fibers at 45 degrees laid in an oblique direction of the engine hood of CFRP on the left direction and the angle of -45 degrees in the right direction were combined. The fibers of [45/-45] were stacked together resulting in an oblique load distribution throughout the area. In addition, it also caused the engine hood of CFRP to collapse very well resulting from the length of the fibers crossed. The fibers had a good deflection when compared to the mean load between aluminum and carbon fiber reinforced plastics with angled fibers at $[0/90]_4$ and $[45/-45]_4$, whereby an increase of 158.12 and 148.79%, respectively, was found while the comparison of the engine hood of $[0/90]_4$ and $[45/-45]_4$ was found to be different by 6.27%.

3.3 Energy absorption

Energy absorption is the amount of energy that a workpiece can absorb during a collision or collapse. This is obtained by summing the area under the graph between the applied load and the time from the collision of the workpiece or structure. It can be seen from Table 6 that when considering the collapse distances of specimens of the same carbon fiber layer characteristics in the FEA model, the angle group [0/90] had a lower collapse value than the [45/-45] and as a result, the energy absorption value of the hood of the group using the [45/-45] fiber arrangement was higher. It was also found that with more layers of carbon fiber, the hood was over-hardened, resulting in less displacement. Even with a higher load value than the number of fibers in 4 layers, the 6 and 8-layer fiber lower the collapsing distance effect was taken into account and the energy absorption was higher than the 4-layer fiber.

The ability to absorb energy was compared between the engine hood of aluminum and carbon fiber reinforced plastics where the absorbed energy was calculated from the mean load multiplied by the collapse of engine hood. From the graph, it was found that the characteristic of the graph tended to increase with an increase in the number of fibers with 4, 6 and 8 layers as shown in Figure 12C. The comparison of the angle influence of fibers between [0/90] and [45/-45] found that the angle of [45/-45] absorbed energy better due to the angle of oblique fibers resulting in a good collapse. The energy absorption ability comparison between aluminum and carbon fiber reinforced plastics with the angles of fibers $[0/90]_4$ and $[45/-45]_4$ showed that the latter could absorb more energy by 29.05 and 35.70%, respectively. In addition, comparing the reinforced plastics with carbon fibers with angles of fibers of $[45/-45]_4$ and $[0/90]_4$ showed that that the former was able to absorb more energy by 22.86%.

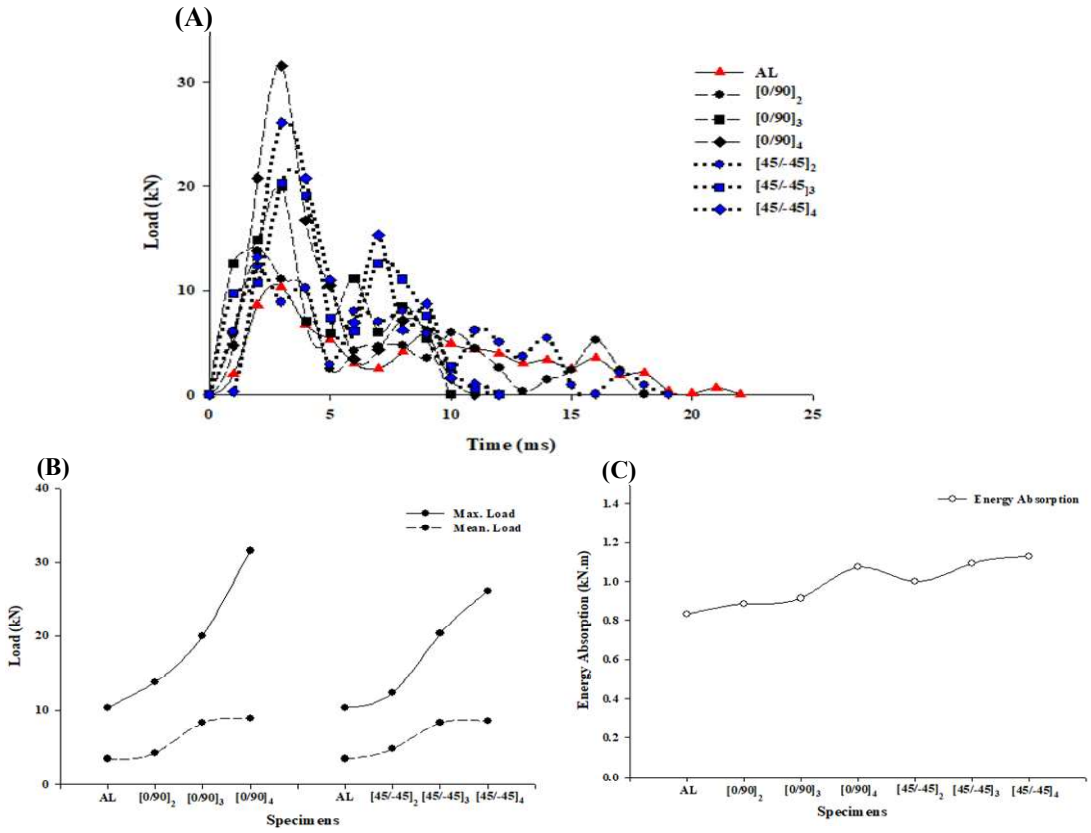

Figure 12 The results from the FEA model (A) the total load and time of the engine hood, (B) the maximum and mean load and (C) the energy absorption.

3.4 Comparison of damage effects

Of the damage that occurred on the various types of hoods, this research focused on the damage pattern of aluminum hood and carbon fiber hood $[0/90]_4$ and $[45/-45]_4$ as shown in Figure 13 due to the 4-layer fiber hood showing the highest energy absorption capability. The von Mises stress distribution showed that the aluminum hood had a greater von Mises stress distribution. Although the maximum von Mises stress value of the aluminum hood was 188.60 MPa, the von Mises stress distribution was found to be higher than that of the carbon fiber hood. The $[0/90]_4$ and $[45/-45]_4$ carbon fiber hoods at a 90-degree fiber angle allowed for a wider distribution of average stress in the transverse direction. The 0-degree carbon fiber angle allowed for better distribution of the average stresses along the longitudinal or vertical hood where the stress band area was 273.7 MPa. In the case of 45-degree carbon fibers, the average stress distribution was wider in the transverse direction. By positioning the carbon fiber angle at 45 degrees, the average stress distribution across the longitudinal or vertical hood resulted in better distribution. The 45-degree carbon fibers served to support and receive the distribution of stress from other fiber layers where the stress bar area was 236.3 MPa.

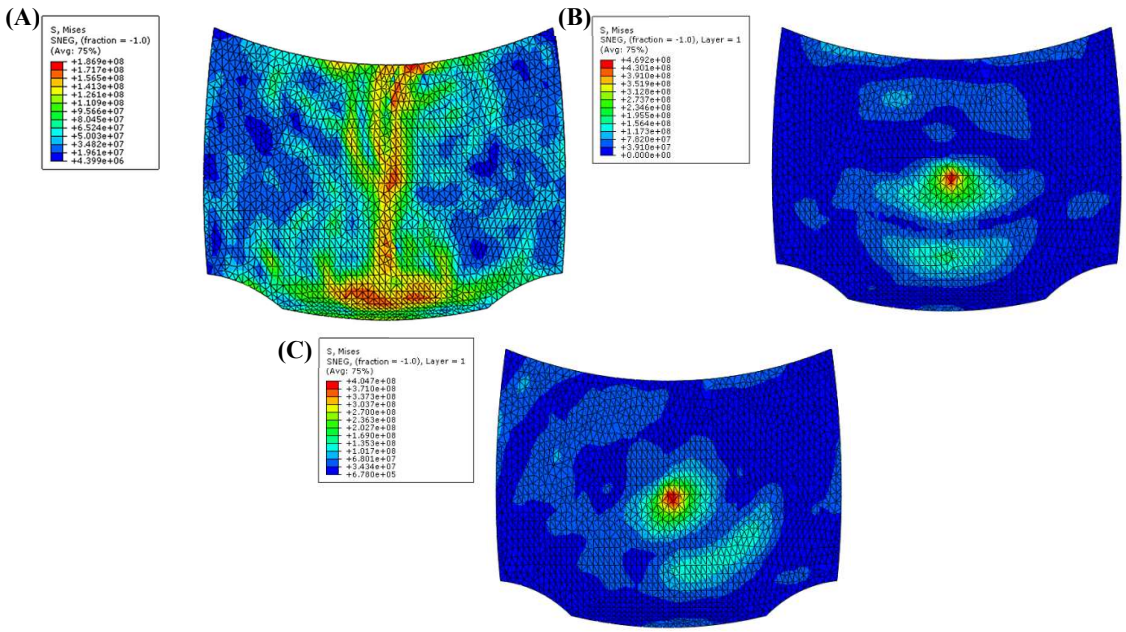

Figure 13 A Comparison of the von Mises stress distribution of (A) the aluminum hood and (B) the $[0/90]_4$ carbon fiber hoods and (C) $[45/-45]_4$ carbon fiber hoods.

4. Conclusion

This research focused on the study of composite materials reinforced with carbon fiber in order to find the ability to absorb energy and strength in automotive parts such as impact resistance and impact strength of materials and can be summarized as follows: 1) The mean load between aluminum and carbon fiber reinforced plastics with fibers angled at $[0/90]_4$ and $[45/-45]_4$ showed an increase of 158.12 and 148.79%, respectively, while the comparison of the engine hood of GFRP at $[0/90]_4$ and $[45/-45]_4$ was found to be different by 6.27%. 2) The energy absorption capacity comparison between aluminum and carbon fiber reinforced plastics with the fiber angles of $[0/90]_4$ and $[45/-45]_4$ showed that the latter could absorb more energy by 29.05 and 35.70%, respectively. In addition, comparing the reinforced plastics with carbon fibers with fiber angles of $[45/-45]_4$ and $[0/90]_4$indicated that the former could absorb more energy by 22.86%.

In terms of commercial applications, it remains to be analyzed as to its cost-effectiveness and economic feasibility. The price of carbon materials in the market is still high. Further studies are needed regarding adding other inexpensive materials to the carbon fiber layer to gain a good impact absorption.

5. Acknowledgements

This research project is supported by Rajamangala University of Technology Isan. Contract No. SKC2562REV030.

6. References

[1] Bajpai P. Chapter 8 - applications of carbon fiber/carbon fiber-reinforced plastic/recycled carbon fiber-reinforced polymers. Car Fiber. 2021:139-155.

[2] Haithem BHF, Leger R, Perrin D, Ienny P, Gerard P, Devaux JF. Recovery and reuse of carbon fibre and acrylic resin from thermoplastic composites used in marine application. Resour Conserv Recycl. 2021;173:105705.

[3] Fernández A, Muro MS, Blázquez FJP, Lopes CS, Aldareguia MJM. Processing and properties of long recycled-carbon-fibre reinforced polypropylene. Compos Part B Eng. 2021;211:108653.

[4] Muda MKH, Mustapha F. Composite patch repair using natural fiber for aerospace applications, sustainable composites for aerospace applications. Sus Compos Aer Appl. 2018;1:171-209.

[5] Wanga F, Zhang Z, Ning F, Wanga G, Dong C. A mechanistic model for tensile property of continuous carbon fiber reinforced plastic composites built by fused filament fabrication. Addit Manuf. 2020;32:101102.

[6] Ghosh T, Kim HC, Kleine RD, Wallington TJ, Bakshi BR. Life cycle energy and greenhouse gas emissions implications of using carbonfiber reinforced polymers in automotive components: front subframe case study. SM&T. 2021;28:e00263.
[7] Das S, Graziano D, Upadhyayula VK, Masanet E, Riddle M, Cresko J. Vehicle light weighting energy use impacts in US light-duty vehicle fleet Sustain. Mater Technol. 2016;8:5-13.
[8] Barnett PR, Hulett BM, Penumadu D. Crashworthiness of recycled carbon fiber composites. Compos Struct. 2021;272:114232.
[9] Wei A, Tan MY, Koay YC, Hu X, Ameri R. Effect of carbon fiber waste on steel corrosion of reinforced concrete structures exposed to the marine environment. J Clean Prod. 2021;316:128356.
[10] Absi C, Alsinani N, Lebel LL. Carbon fiber reinforced poly(ether ether ketone) rivets for fastening composite structures. Compos Struct. 2022;280:114877.
[11] Soutis C. Carbon fiber reinforced plastics in aircraft construction. Mater Sci Eng. 2005;412(1-2):171-176.
[12] Chowdhury NM, Chiu WK, Wang J, Chang P. Experimental and finite element studies of bolted, bonded and hybrid step lap joints of thick carbon fibre/epoxy panels used in aircraft structures. Compos Part B Eng. 2016;100:68-77.
[13] Torkestani A, Sadighi M, Hedayati R. Effect of material type, stacking sequence and impact location on the pedestrian head injury in collisions. Thin-Walled Struct. 2015;97:130-139.
[14] Ahmed A, Wei L. Introducing CFRP as an alternative material for engine hood to achieve better pedestrian safety using finite element modeling. Thin-Walled Struct. 2016;99:97-108.
[15] Kim DH, Jung KH, Kim DJ, Park SH, Kim DH, Lim JY, et al. Improving pedestrian safety via the optimization of composite hood structures for automobiles based on the equivalent static load method. Compos Struct. 2017;176:780-789.
[16] Huang S, Yang J. Optimization of a reversible hood for protecting a pedestrian's head during car collisions. Accid Anal Prev. 2010;42:1136-1143.
[17] Mamalis D, Floreani C, Brádaigh CMO. Influence of hygrothermal ageing on the mechanical properties of unidirectional carbon fibre reinforced powder epoxy composites. Compos Part B Eng. 2021;225:109281.
[18] Ueda M, Tasaki Y, Kawamura C, Nishida K, Honda M, Hattoric K, et al. Estimation of axial compressive strength of unidirectional carbon fiber reinforced plastic considering local fiber kinking. Compos Part C Open Access. 2021;6:100180.
[19] Junchuan V, Thinvongpituk C. The Influence of fiber orientation and stacking sequence on the crush behavior of hybrid AL/GFRP tubes under axial impact. Mater Trans. 2020;61(7):1322-1331.
[20] ASTM International [Internet]. Pennsylvania: The Organization; c1996-2023 [cited 2021 Dec 14]. ASTM D3039/D3039 M-17: standard test method for tensile properties of polymer matrix composite materials. Available from: https://www.astm.org/d3039_d3039m-17.html.
[21] Deck C, Willinger R. Improved head injury criteria based on head FE model. Int J Crashworthiness. 2008;13(6):667-678.
[22] Sellitto A, Riccio A, Magno G, Errico G, Monsurro G, Cozzolino A. Feasibility study on the redesign of a metallic carhood by using composite materials. Int J Automot Technol. 2020;21(2):471-479.
[23] Acanfora V, Saputo S, Russo A, Riccio A. A feasibility study on additive manufactured hybrid metal/composite shock absorbers. Compos Struct. 2021;268:113958.